Available online at www.sciencedirect.com

ScienceDirect

Solid Earth Sciences 6 (2021) 12–26

www.elsevier.com/locate/SESCI

Using computer-aided image processing to estimate chemical composition of igneous rocks: A potential tool for large-scale compositional mapping

Julin Zhang*, Cin-Ty A. Lee, Michael Farner

Department of Earth, Environmental and Planetary Sciences, Rice University, Houston, TX, United States

Received 19 October 2020; revised 10 December 2020; accepted 13 December 2020
Available online 27 February 2021

Abstract

Digital cameras, particularly on smartphones, have led to the proliferation of amateur photographers. Of interest here is the use of smartphone cameras to conduct rapid, low-cost compositional mapping of geologic bedrock, such as plutons and batholiths, in combination with chemical analyses of rocks in the laboratory. This paper discusses some of the challenges in geochemical mapping using image analysis. We discuss methods for color calibration through a series of experiments under different light intensities and conditions (spectra). All indoor and outdoor experiments show good reproducibility, but suffer from biases imparted by different light intensities, light conditions, and camera exposure times. These biases can be greatly reduced with a linear color calibration method. Over-exposed and under-exposed images, however, cannot be fully calibrated, so we discuss methods that ensure images are properly exposed. We applied our method to 59 natural granitoid and mafic enclave samples of known chemical composition. Multivariate linear regression has been explored for relating calibrated rock images with chemical compositions. Among all the chromatic and texture features of rock images, we show that average gray levels strongly correlate with major oxide concentrations. Subtle variations in bulk composition can potentially be rapidly assessed using calibrated photographs of outcrops.

Keywords: Mapping; Image processing; Color calibration; Geochemistry

1. Introduction

There is a growing need for rapid, large-scale compositional mapping of outcrops and land surface as the pressures for mineral exploration and environmental assessment grow. The most accurate approach for compositional mapping is to collect samples from the field and analyze them in the laboratory through various geo-analytical methods (X-ray fluorescence, inductively coupled plasma mass spectrometry, etc.), but these approaches are too expensive and too slow to fully support rapid, large-scale compositional mapping (Potts, 2012). There is thus a need to explore other methods that may be less precise but compensate for this deficiency by allowing for the accumulation of large datasets. The best trained geologists serve as walking image processors and analyzers as they are trained to identify rocks and interpret their origins from rock textures and colors based solely on the unaided eye and years of experience. Human eyes and brains are not the same, so considerable observer variability and bias is introduced when more than one geologist is conducting a lithological survey. Computer-aided processing of rock textures has thus become an important part of quantifying such quantities as grain size, shape and spatial distribution in igneous and metamorphic petrology (Åkesson et al., 2003; Cashman and Ferry, 1988; Cashman and Marsh, 1988; Heilbronner, 2000; Jerram et al., 2003; Kemeny et al., 1993).

In this paper, we explore the use of color and grayscale in quantifying the composition of plutonic igneous rocks. Because color can correlate with mineralogy, it might be expected to correlate with composition within a certain group of geologic materials. There are, however, many challenges in

* Corresponding author.
E-mail address: zhangjulin89@gmail.com (J. Zhang).
Peer review under responsibility of Guangzhou Institute of Geochemistry.

https://doi.org/10.1016/j.sesci.2020.12.003

using color quantitatively because many variables control color and its perception (Stevens et al., 2007). For example, alteration can easily modify the surface color of mineral grains. In addition, apparent color varies depending on the spectrum of light, which can change throughout the day or under different lighting conditions (Foster, 2011; Romero et al., 2003). There is thus a need for robust color calibration, particularly if color is being assessed outdoors when conditions change continually. In the soil science community, eye-based side-by-side comparison with the Munsell color chart has been widely used to quantify soil color in the field (Color, 2015; Pendleton and Nickerson, 1951; Rossel et al., 2006). Similar computer-based calibration against color guides (Joshi and Jensen, 2004; Pascale, 2006) has been applied to problems in food science, biosciences, agriculture and planetary exploration (Allender et al., 2018; Costa et al., 2010; Fischer, 2019; Wu and Sun, 2013).

We note that the development of plant and animal identification algorithms in mobile phone apps has decreased the barriers for citizens to report observations, resulting in the largest and most comprehensive biodiversity survey of the planet to date, a feat that could never have been accomplished by all living scientists combined (Sullivan et al., 2014; Van Horn et al., 2018). In the Earth science community, a mobile app named StraboTools has recently been developed for quantifying field observations of textural features, such as foliation, mineral alignment and mineral proportion (Glazner and Walker, 2020), opening up an opportunity for large-scale, high resolution mapping using citizen science. StraboTools also incorporates color, but a number of calibration issues persist when estimating color from natural samples. Here, we develop a method for calibrating and quantifying color from images taken from simple hand-held digital cameras or phone cameras. Our method can help geologists accumulate and report color-calibrated rock images, contributing to the buildup of a color-calibrated rock image database. Like the widespread geochemical database such as GeoRoc and EarthChem, this rock image database may provide another opportunity for using big data to solve earth science problems. One promising long-term goal is to map out compositional variations of a pluton on the scale of meters or less with color and texture-based image analysis, helping us better understand the dynamics of magmatic systems. In this paper, we focus on the color consistency of rocks under different ambient light conditions, which is a small step towards that goal. It is the hope that subtle variations in composition can be detected by quantifying subtle variations in color.

2. Material and methods

2.1. Samples

Image analyses were conducted on felsic granitoids and mafic enclaves from the Bernasconi Hills pluton, northern Peninsular Ranges Batholith in California, USA (Farner et al, 2014, 2018). These samples consist primarily of quartz and plagioclase with small amounts of hornblende and biotite. Felsic or silicic minerals, such as quartz and plagioclase, appear as transparent or white, whereas mafic or dark minerals like hornblende and biotite are dark brown to black. In this study, we will estimate two useful indices, the average gray level and relative proportion of dark minerals, that may relate to the chemical compositions of rocks, and in particular, to explore the challenges of quantifying these two indices under variable lighting conditions.

2.2. Experimental setup

We first conducted a series of indoor experiments under controlled light conditions to gain a sense of how ambient light affects perceived color. In all experiments, we used an iPhone 7 Plus digital camera with an aperture of f/1.8. For indoor lighting, we used two TaoTronics™ LED table lamps (12 W and 410 lumens). These LED table lamps have 5 lighting conditions (cold white - CW, white - W, natural - N, yellow -Y and warm yellow - WY) and 7 intensity levels where level 1 refers to the lowest intensity and level 7 for highest intensity. The two LED lamps were placed 26 cm over the sample and with a separation distance between the two lamps of 23 cm to minimize shadows (Fig. 1a). The camera was placed slightly higher than the lamps to avoid generating shadows (Fig. 1a). A phone holder and camera shutter remote control were used to avoid vibrations.

In order to calibrate color, we placed an X-Rite ColorChecker Passport™, which has 24 pure color patches with known sRGB values, adjacent to the rock sample for all photographs (Fig. 1b). sRGB is short for standard Red Green Blue and is one of the most common color spaces. sRGB uses the combinations of three primary colors (red, green and blue) with varying amounts to simulate most colors. Instead of using the default camera application in the iPhone 7 Plus, which stores images in the form of JPEGs, photographs were taken using an app called Camera+™. Camera+™ stores images in DNG format, which is a raw file format that does not normalize the spectral histogram of an image. Camera+™ also allows the option to manually change camera settings, such as exposure time and ISO, etc. However, for indoor experiments, we used auto mode, which allows the program to automatically choose the proper exposure time and ISO.

Image experiments were also performed outdoors under natural daylight conditions. Due to the high intensity of daylight and the ease to which iPhone cameras become saturated, pictures taken with an iPhone under bright daylight are usually overexposed, making it difficult if not impossible to calibrate an overexposed image. To solve this problem, we attached a PolarPro™ Iris neutral density filter (ND filter) in front of the camera lens. We used the ND8 filter, which reduces the amount of incident light by a factor of 8 but does not change the spectrum of the incident light. Unlike the auto mode choice for indoor experiments, we manually set the exposure time and ISO for outdoor experiments and explored the effect of camera settings on the performance of the calibration.

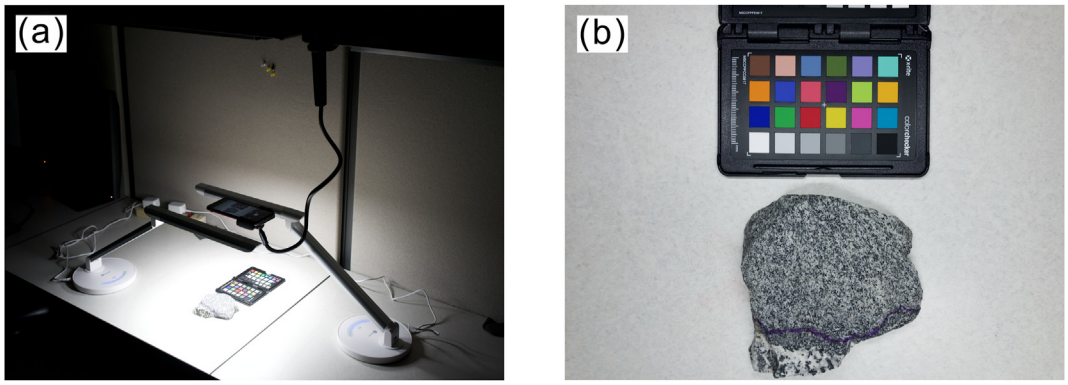

Fig. 1. Indoor experiment environment and materials used in this project. (a) Two LED lamps were placed in parallel over the sample. An iPhone was placed above the lamps. (b) A mafic enclave sample, along with a color checker, was placed under the lamps.

2.3. Calibration method

Luminosity calibration is usually required before color calibration to compensate for spatially heterogeneous transmission of light across the camera lens area (Hong et al., 2001; Losey, 2003). We used a white calibration board on the X-Rite ColorChecker Passport™ to check for spatial homogeneity of luminosity distribution by placing the whiteboard in the same positions where the sample and the color checker would sit. The same camera settings were adopted for all photographs (exposure time of 1/120 s and ISO of 25). Our results show that the gray level histograms of the two areas (sample and color checker) were very similar, with mean grayscale values within 2% (Fig. 2a and b). There was thus no need to perform any luminosity calibrations before color calibrations. In the field, so long as the light source is diffuse on the length scale of the sample, luminosity corrections are not needed.

Color was calibrated with the X-Rite ColorChecker Passport™, which offers 24 color patches with known sRGB values. RGB measurements of each of the 24 color patches were mapped to the 'real' RGB tristimulus values (the values of red, blue and green channels) to develop a calibration model for each photograph. A linear model shown below was assumed:

$$Red_{calib} = \alpha_0 + \alpha_1 * Red + \alpha_2 * Green + \alpha_3 * Blue$$

$$Green_{calib} = \beta_0 + \beta_1 * Red + \beta_2 * Green + \beta_3 * Blue$$

$$Blue_{calib} = \gamma_0 + \gamma_1 * Red + \gamma_2 * Green + \gamma_3 * Blue \quad (1)$$

where Red_{calib}, $Green_{calib}$ and $Blue_{calib}$ refer to the red, green and blue values of a patch on the color checker after calibration, *Red*, *Green* and *Blue* represent the RGB measurements of that patch before calibration, and α, β and γ are the parameters of the model. These parameters are determined by minimizing the total discrepancy between measured RGB tristimulus values of these 24 patches and their corresponding standard values. The smaller the total discrepancy is, the better the fit will be for the color checker. It is assumed that this mapping function derived from the color checker is valid for our rock samples.

The color histogram is an important feature of an image since it represents the distribution of colors in the image. Therefore, in this study we are also interested in studying the

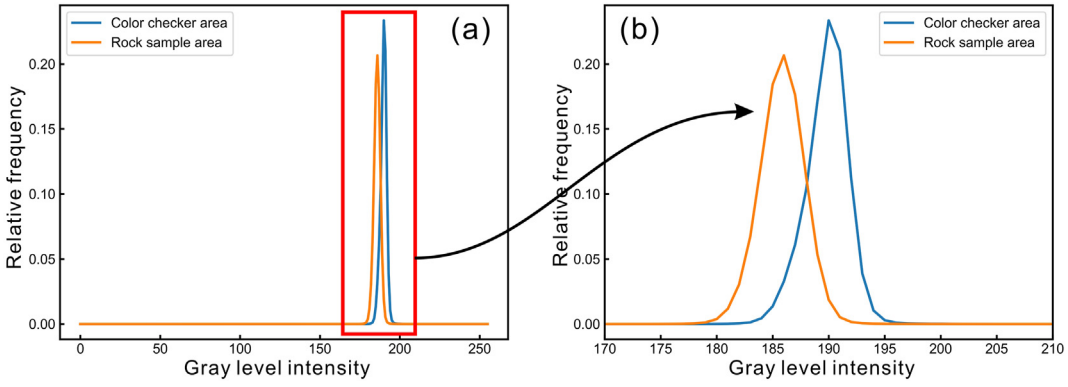

Fig. 2. Results of luminosity experiments. (a) Comparison of two gray level histograms of the same whiteboard placed at the positions where the sample (orange histogram) and the color checker (blue histogram) should sit. (b) Zoomed in view of (a). Gray level mean for sample and color checker locations are ~185 and ~190, respectively.

histogram consistency of images before and after color calibration. Because the colors of minerals in our rock samples are primarily black and white, we studied the gray level histogram of the images instead of three separated RGB histograms. The algorithm of converting RGB tristimulus values of a pixel in the sRGB color space to one gray level value used in this paper follows the ITU-R Recommendation BT.601, which specifies methods for digitally coding video signals (BT, 2011):

$$Gray = Red^{*}0.299 + Green^{*}\,0.587 + Blue^{*}0.114 \quad (2)$$

2.4. Feature extraction from histograms

The gray level histogram of the rock image is assumed to be a mixture of two signals, each of which represents the signal of a dark or light mineral group. These two signals can be segmented by the Otsu thresholding algorithm (Otsu, 1979). The dark and light mineral proportions were then estimated based on the binarization result. In addition, the average gray level intensity of histograms, which evaluate the overall gray level intensity of the rock image, also was considered in this study. All the programs in this study were coded in Python 3.6 (code can be accessed via https://github.com/Zhangjulin/Color_calibration/blob/master/Color_calibration.py).

3. Results

3.1. Reproducibility of indoor and outdoor experiments

In order to evaluate internal reproducibility, images of a same rock sample along with the color checker (Fig. 1b) were taken 10 times under the same light condition. We checked the consistency of gray level histograms among these 10 images before and after color calibration. The reproducibility experiments were done both indoor and outdoor. For the indoor reproducibility experiments, two LED lamps were set to white (W) light condition and intensity level of 5. Auto mode on the iPhone was used, resulting in an exposure time of 1/300 and ISO of 25. For the outdoor reproducibility experiments under daylight, we attached an ND8 filter to the iPhone camera to avoid overexposure and we manually set the exposure time to 1/750 and ISO to 25.

The results show that both indoor and outdoor histograms have good internal consistency before and after color calibration (Fig. 3). We note that there is a small spike at gray level intensity of 0 in the outdoor non-calibrated histograms (Fig. 3c), indicating a slight underexposure. In any case, histograms are bimodal with the left peak representing the dark mineral mode and the right peak representing the light mineral mode. These two modes overlap between gray level intensity 60 to 130.

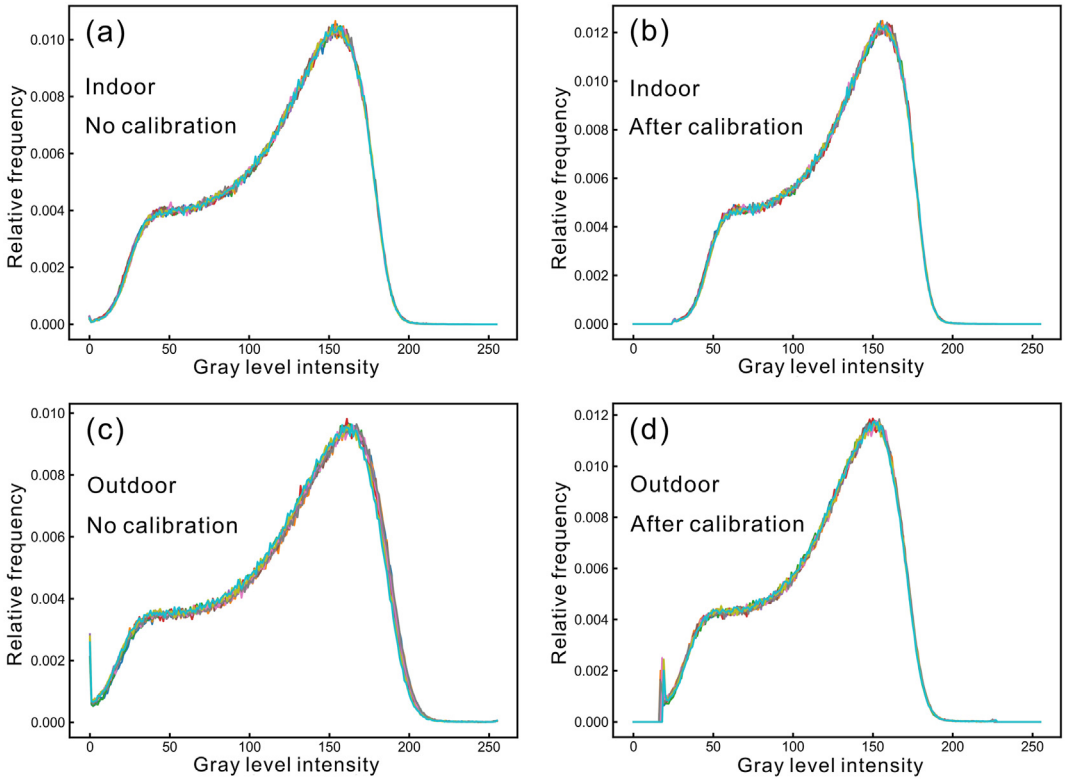

Fig. 3. Results of reproducibility experiments. (a) Indoor result before calibration, (b) indoor result after calibration, (c) outdoor result before calibration and (d) outdoor result after calibration. Each panel shows the results of 10 independent experiments.

Average gray level intensities and mineral proportions were later determined from calibrated histograms. We also evaluated the reproducibility of these two indices. The results show that the mean value of dark mineral proportion for indoor experiments is 0.365 with a relative two standard deviation (2RSD) of 1.54% while the mean and 2RSD for outdoor experiments are 0.354 and 0.680% (detailed data can be found in the supplemental materials). The mean and 2RSD of dark mineral proportions between indoor and outdoor experiments were similar. The average gray level for indoor experiments is 125.2 (2RSD = 0.12%) and 117.2 (2RSD = 0.22%) for outdoor experiments.

3.2. Indoor experiments

We accumulated 35 images of the same rock sample (Fig. 1b) indoors with different LED light conditions or intensities. The results show that light conditions and intensities significantly influence image colors. Two representative rock images taken under different conditions are shown in Fig. 4: one was taken under CW light condition with intensity level of 2 (Fig. 4a) and the other under WY light condition with intensity level of 6 (Fig. 4b). The uncalibrated images show differences in yellow hues, but are consistent with each other after calibration (Fig. 4c and d), validating our color calibration method.

We also checked the consistency of gray level histograms for all 35 rock images. The gray level histograms of these images after color calibration show more internal consistency than before color calibration (Fig. 5). The discrepancy of uncalibrated histograms is due to differences in LED light conditions and intensities. More results and discussions about the influence of light conditions and intensities on image colors are in the Appendix.

Average gray levels and mineral proportions were estimated from both uncalibrated and calibrated histograms. The mean value of average gray levels of uncalibrated histograms is 115.0 (2RSD = 6.2%) and that of calibrated histograms is 125.3 (2RSD = 0.78%). The mean value of calibrated results is ~9% larger than that of the uncalibrated results, and the variance of calibrated results is much smaller. The mean value of the dark mineral proportions estimated from uncalibrated histograms is 0.359 (2RSD = 2.68%), and 0.360 (2RSD = 2.80%) for calibrated histograms. The mineral proportions estimated from uncalibrated and calibrated histograms are similar. While the mean values of average gray levels and dark mineral proportions are similar for different light conditions, there is more variation in the magnitude of the 2RSDs across light conditions (Table 1). CW light displays the largest variability whereas WY light displays the smallest variability, with 2RSD decreasing as the softness of light increases.

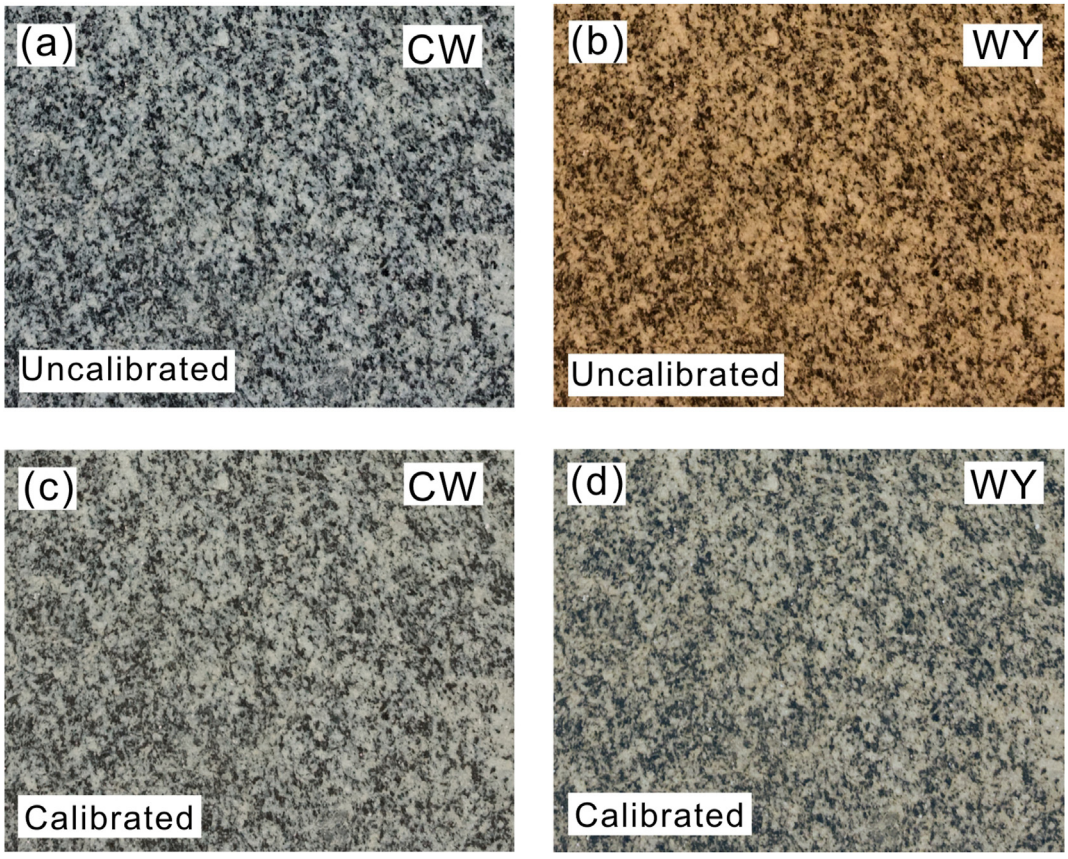

Fig. 4. RGB images of the rock sample taken under (a) CW light condition with intensity level of 2 before calibration, (b) WY light condition with intensity level of 6 before calibration, (c) CW light condition with intensity level of 2 after calibration, and (d) WY light condition with intensity level of 6 after calibration.

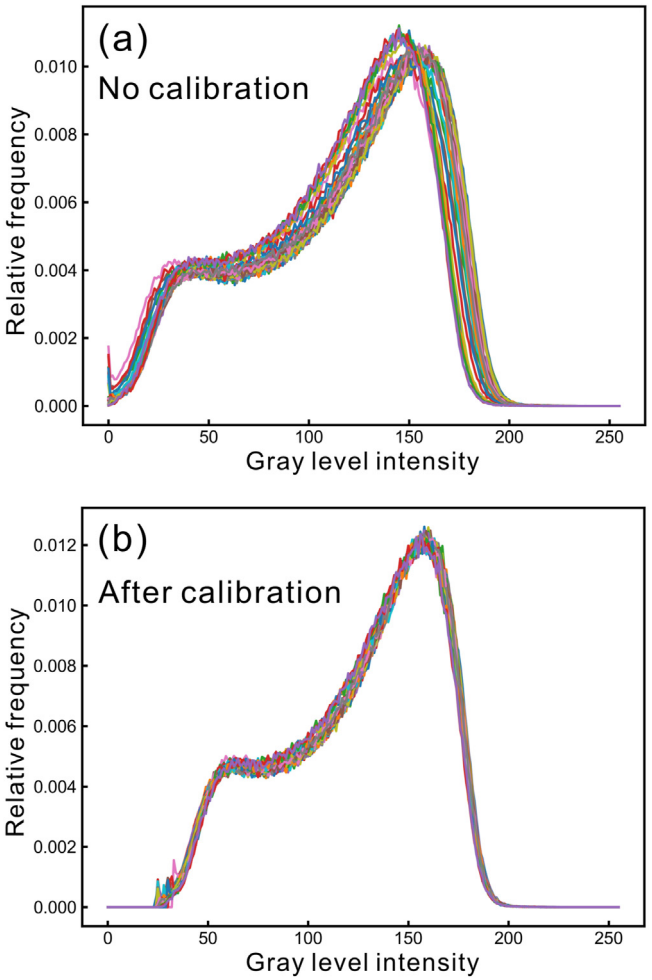

Fig. 5. Gray level histograms of the same rock sample under different indoor LED light conditions and intensities. (a) Histograms before color calibration and (b) histograms after color calibration.

For comparisons, we also applied the built-in color index (CI) tool in StraboTools (Glazner and Walker, 2020). StraboTools allows users to highlight the desired pixels by using a slider to manually set the threshold, providing another way to estimate the dark mineral proportion. Here, we compare the results between the StraboTools CI function and the Otsu method used in this study. A representative color-calibrated gray level rock image, taken under N light condition and light intensity level of 4, has been used for the comparison (Fig. 6a). The dark mineral pixels are highlighted in red (Fig. 6b and c). Using StraboTools and manually setting the threshold based on visual inspection, we find that the StraboTools dark mineral proportion is within error of the Otsu method (Fig. 6b and c). However, we emphasize that our automated algorithmic approach ensures consistency between observers. Relying on manual threshold setting may introduce uncertainties associated with observer bias.

Table 1
Average gray levels and dark mineral proportions estimated from calibrated histograms under different light conditions.

Light condition	Average gray level		Dark mineral proportion	
	Mean	2RSD	Mean	2RSD
Cold white (CW)	125.2	0.59%	0.357	3.95%
White (W)	125.4	0.42%	0.358	1.81%
Natural light (N)	125.6	0.27%	0.357	1.29%
Yellow (Y)	125.7	0.16%	0.359	1.75%
Warm yellow (WY)	124.5	0.18%	0.366	0.491%
All	125.3	0.78%	0.360	2.80%

3.3. Outdoor experiments under uncontrolled daylight

In order to study the influence of dynamic daylight in gray level histograms, we conducted 20 series of outdoor experiments at different times of the day (from morning to afternoon) and on days with different light conditions (sunny and cloudy days).

Here, we present the results of one representative outdoor experiment performed on a sunny afternoon. We first explored auto mode (exposure time of ~1/3500 and ISO of 20). Every data point in Fig. 7a represents red (green or blue) measurements corresponding to the 24 calibration standards. Nearly all RGB measurements of the color checker deviate positively from the standard values (Fig. 7a). Some RGB measurements even approach the saturation limit (255), which indicates overexposure. The uncalibrated histogram under auto mode shifts much lighter compared to indoor uncalibrated histograms as exemplified in Fig. 7b for N light condition and intensity level of 4. A linear color calibration was found to fix the shift but there remains obvious discrepancy between the histogram shape, especially towards the dark mineral mode (Fig. 7c).

To improve on this, we attached an ND8 filter to the iPhone 7 Plus, which reduces the amount of light transmitted to the camera. Images were taken with a series of different exposure times (1/500, 1/750, 1/1000 and 1/1500) with ISO manually fixed to 25 to be consistent with the indoor experiments. The exposure time of 1/500 combined with an ND8 filter still results in overexposure and does not improve results (Fig. 7d–f). When the exposure time decreases to 1/750 and 1/1000, the discrepancy between measurements and standards in the color checker are reduced, and both the uncalibrated and calibrated histograms match better with reference histograms (Fig. 7g-l). However, when exposure time decreases to 1/1500, all the RGB measurements fall below the corresponding standards due to underexposure (Fig. 7m). This underexposure drives the uncalibrated histogram to shift darker (Fig. 7n) and worsens the calibrated histogram (Fig. 7o). These results show that a too small or too large exposure time will distort the histogram even after calibration. Therefore, an optimal exposure time window is necessary, and for this outdoor experiment, exposure time of 1/750–1/1000 is favored.

The results of other 19 outdoor experiments show that the optimal exposure time varies under different daylight conditions (see supplemental material). Average gray levels and dark mineral proportions of the 20 outdoor experiments were determined from calibrated histograms that were properly exposed. The mean value of average gray levels for these 20

experiments is 115.5 (2RSD = 4.3%, Table 2). The outdoor mean value is ~8% lower than the indoor result (125.3, 2RSD = 0.78%) and has a larger 2RSD. The mean value of dark mineral proportions is 0.365 (2RSD = 8.07%), which is close to the indoor result (0.360, 2RSD = 2.80%) but has a larger 2RSD. Without the assistance of a ND filter, both the average gray level (115.9, 2RSD = 6.0%) and mineral proportion estimates (0.339, 2RSD = 18.6%) exhibit much larger variation (Table 2).

4. Discussion

4.1. Prospects and pitfalls of imaging

The reproducibility tests show that an iPhone 7 Plus, combined with the Camera+ app, can obtain consistent gray level histograms under the same light condition (Fig. 3a, c). The linear color calibration method maintains this consistency even though histogram shapes are changed (Fig. 3b, d). Limited variation of average gray level and dark mineral proportions estimated from calibrated histograms indicate that our method is robust.

Indoor experiments show that varying light conditions impact color information (Fig. 4a and b). Differences in the light condition or intensity can lead to inconsistency of gray level histograms on the same rock sample (Fig. 5a). However, we showed that consistency can be improved significantly with a linear calibration (Fig. 4c and d, Fig. 5b), supporting the validity of our method to calibrate histograms under indoor conditions. Outdoor experiment results show that auto mode is very likely to overexpose images (Fig. 7a and b). We also show that a linear calibration cannot perfectly calibrate the histograms (Fig. 7c). Therefore, for field geological mapping, it is wise to use manual mode with an ND filter and set proper exposure time appropriate to the daylight condition (Fig. 7d-o).

Average gray level and dark mineral proportion were determined from the histograms. Overall, these two indices of indoor experiments vary much smaller than outdoor experiments (Table 2). This may due to the uncontrolled property of daylight. Indoor experiment results show that the average gray level of calibrated histograms has a much smaller variation (2RSD = 0.78%) than uncalibrated histograms (2RSD = 6.2%). This means that calibration can greatly improve the consistency of the average gray level under different light conditions. The dark mineral proportion results between calibrated and uncalibrated histograms are similar. This is because within the variability of indoor light conditions, calibration does not significantly change the shapes of the histograms which determine the Otsu thresholding results. In contrast, for the outdoor experiments without the ND filter, calibration significantly changes the shapes of histograms (Fig. 7c). Therefore, the dark mineral proportion results (0.339, 2RSD = 18.6%) are not consistent well with the indoor experiments (0.360, 2RSD = 2.80%, Table 2). The much better result of proper exposed outdoor experiments with an ND filter

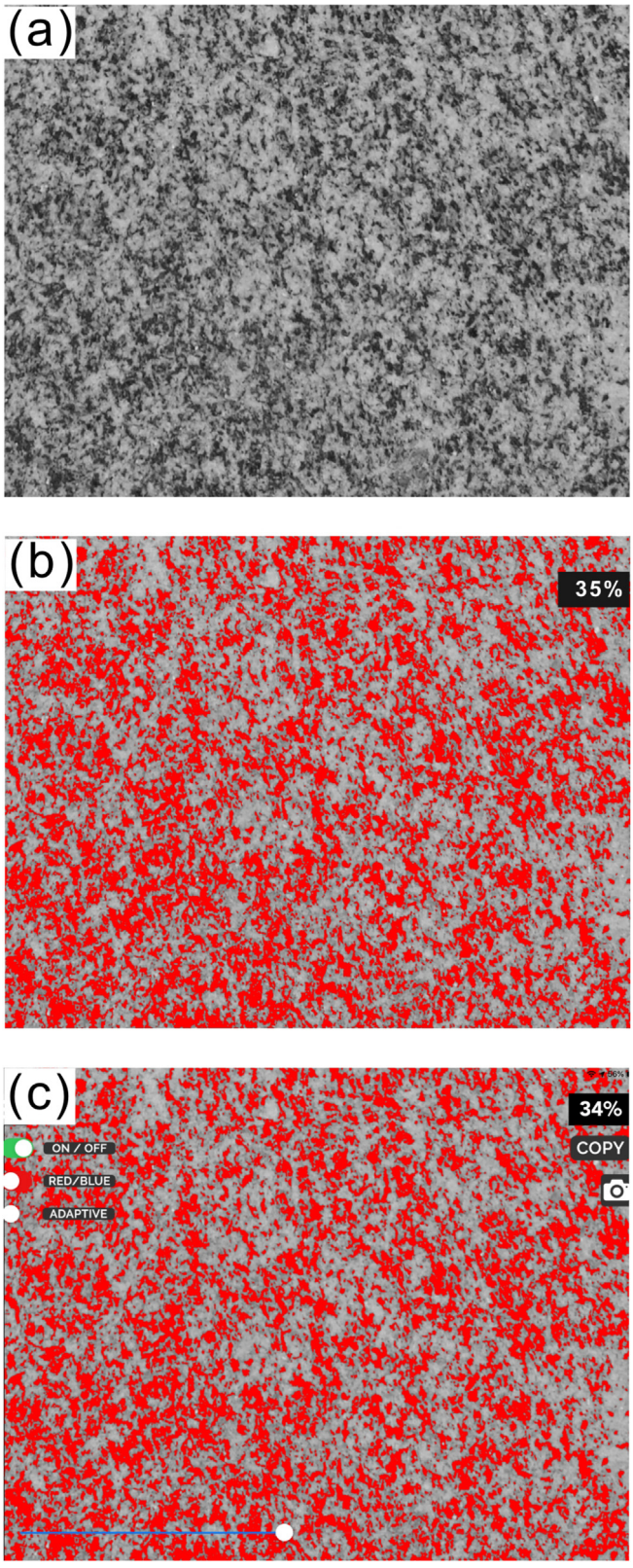

Fig. 6. A comparison of the dark mineral proportion estimates between the Otsu method and color index (CI) tool in the StraboTools. (a) A representative rock image taken under N light condition and light intensity level of 4. Dark mineral proportions determined from (b) Otsu method and (c) CI tool. Dark mineral pixels are highlighted in red.

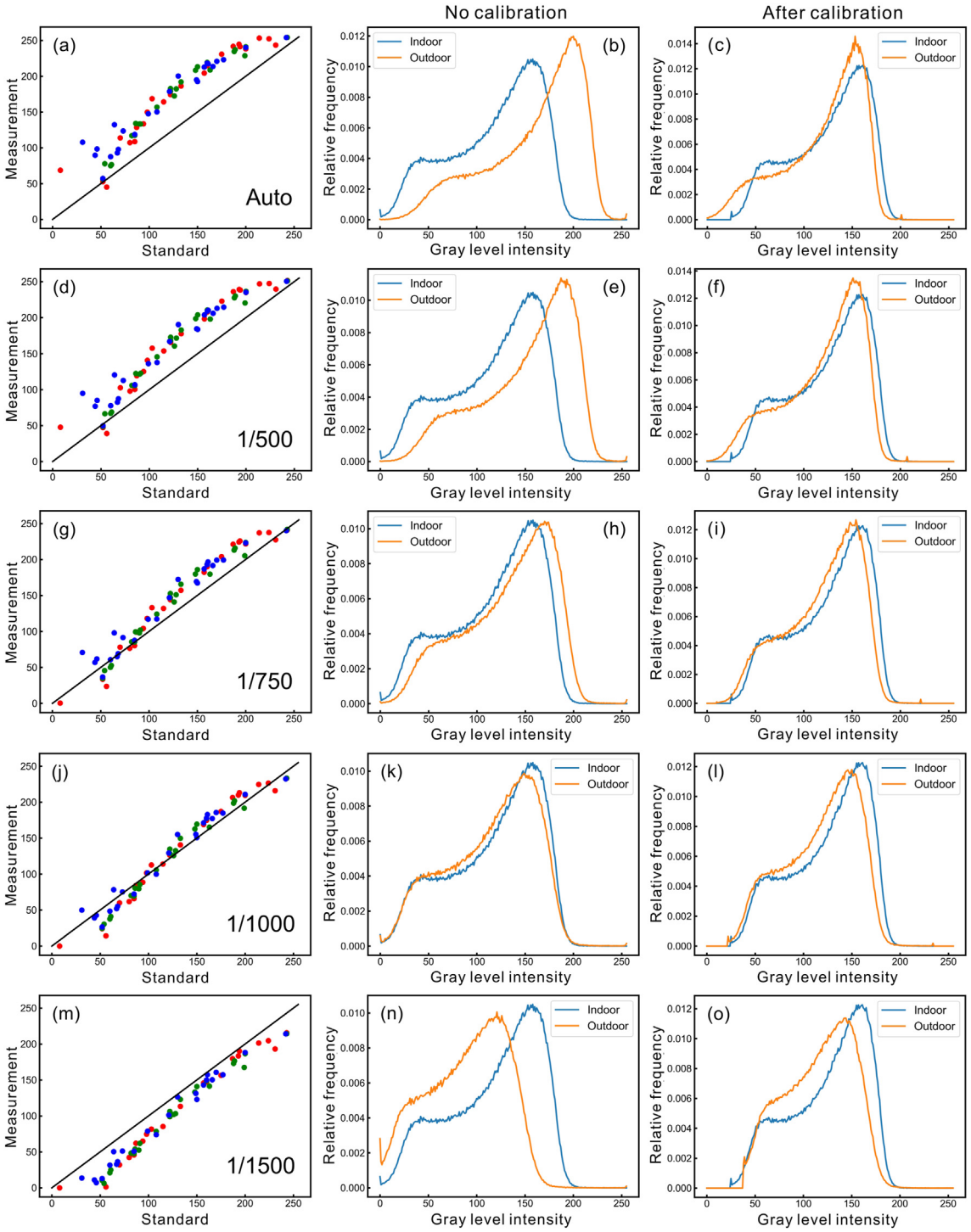

Fig. 7. Outdoor color calibration results with different exposure times. (a) Comparison of the measured RGB values to standard values of the color checker, (b) uncalibrated and (c) calibrated histograms of the rock sample when using auto exposure. The results when manually setting the exposure time to (d)–(f) 1/500, (g)–(i) 1/750, (j)–(l) 1/1000 and (m)–(o) 1/1500 s.

(0.365, 2RSD = 8.07%, Table 2) supports the necessity of an ND filter under daylight conditions.

The advantage of our method is that it is simple, quantitative and objective, and eliminates biases between multiple observers or inconsistencies within an individual observer. However, there are some limitations. In addition to the varying light conditions and intensities, weathering of surfaces in the field can bias the color of rocks. The roughness of rock surfaces can also influence the average grey level due to shadows and reflections (Adams and Filice, 1967).

Table 2
Average gray levels and dark mineral proportions estimated from calibrated histograms indoors and outdoors.

Indoor/Outdoor	*ND filter*	*Average gray level*		*Dark mineral proportion*	
		Mean	2RSD	Mean	2RSD
Indoor	No	125.3	0.78%	0.360	2.80%
Outdoor	Yes	115.5	4.3%	0.365	8.07%
Outdoor	No	115.9	6.0%	0.339	18.6%

4.2. Application to petrology

Many studies have explored the use of chromatic features and/or textural features to classify rocks (Bianconi et al., 2012; Doğan and Akay, 2010; Ershad, 2011; Ferreira and Giraldi, 2017; Gökay and Gundogdu, 2008; Kurmyshev et al., 2003; Lepistö et al., 2005; Perez et al., 2015; Ran et al., 2019; Topalova and Tzokev, 2010). However, few studies attempted to quantitatively link such features to chemical composition (Kemp, 2014). We performed indoor experiments on 59 rock samples for which bulk chemical compositions were analyzed by XRF. These rocks are from the Bernasconi Hills pluton in the northern Peninsular Ranges Batholith in California, USA (Farner et al, 2014, 2018). Thirty-five of these samples are felsic granitoids and the remaining are mafic enclaves. Only the fresh faces of rock samples were used here since weathering can cause discoloration of mineral surfaces. We followed our indoor protocols outlined above. Rock samples were placed under two LED lamps along with a color checker for color calibration. All 59 experiments were carried out under N light condition and light intensity level of 4.

Both the chromatic features and textural features were considered for predicting the chemical composition of rocks. To extract the chromatic features of rock images, we converted the original RGB color space to HSI color space, which provides a more intuitive way to describe the color. Another advantage of HSI color space is that it separates the chromatic information from the luminance information. HSI color space consists of three components: hue (H), saturation (S) and intensity (I). Hue (H) represents color and saturation (S) is the dominance of hue in color. These two are the chromatic components. Intensity (I) is the luminance component that represents the brightness or darkness of the color, similar to gray level intensity. The conversion to HSI color space from RGB color space is given below:

$$H=\begin{cases} cos^{-1}\left(\dfrac{(R-G)+(R-B)}{2\sqrt{(R-G)^2+(R-B)(G-B)}}\right), \ if\ B\le G \\ 2\pi - cos^{-1}\left(\dfrac{(R-G)+(R-B)}{2\sqrt{(R-G)^2+(R-B)(G-B)}}\right), if\ B>G \end{cases}$$

$$S=1-\frac{3*\min(R,G,B)}{R+G+B}$$

$$I=\frac{R+G+B}{3} \quad (3)$$

In this study, the average and standard deviation of hue and saturation of rock images are referred to as chromatic features. The average and standard deviation of gray level (or intensity) are luminance features. Textural analysis is based on a gray level co-occurrence matrix (Arvis et al., 2004; Haralick et al., 1973; Partio et al., 2002), which is a classical second-order statistical method that measures how often different pairs of two pixels co-occur in a gray level image. Every element $p(i,j)$ in this matrix represents the frequency of two neighboring pixels, one having gray level i and the other one having gray level j, occurring in the image at a given offset. The co-occurrence matrix depends on the offset, and in general, horizontal, vertical and diagonal offsets are favored. In this study, we considered all of them and followed eight directions: {0°, 45°, 90°, 135°, 180°, 225°, 270°, 315°} The grayscale of rock images is 0–255, so the size of the co-occurrence matrix in this study is 256*256.

Four popular textural features were extracted from the co-occurrence matrix: contrast (C), correlation (Corr), energy (E) and homogeneity (Hom).

$$C=\sum_{i,j}(i-j)^2*p(i,j)$$

$$Corr=\sum_{i,j}\frac{(i-\mu_i)*(j-\mu_j)*p(i,j)}{\sigma_i*\sigma_j}$$

$$E=\sqrt{\sum_{i,j}p(i,j)^2}$$

$$Hom=\sum_{i,j}\frac{p(i,j)}{1+(i-j)^2} \quad (4)$$

where contrast measures the amount of local variance; correlation measures linear dependency of gray levels of two neighboring pixels over the whole image, μ_i is horizontal mean and σ_i is horizontal variance of the co-occurrence matrix while μ_j and σ_j are vertical mean and vertical variance, respectively; energy refers to the extent of textural uniformity; homogeneity quantifies the local homogeneity and reaches its maximum when all the pixels in the image have the same gray level. All the texture features are normalized to [0,1] in this study.

The preliminary exploration shows that the average gray levels of calibrated histograms correlate well with some chemical components (Fig. 8a–c). The average gray level correlates negatively with FeO and CaO, and positively with SiO_2. We attribute this to the fact that the most abundant

dark mineral in these samples is hornblende, which is rich in Fe and Ca. For FeO, correlation coefficients R^2 with average gray level are up to 0.90 (Fig. 8a), and for SiO_2 and CaO are 0.83 and 0.77, respectively (Fig. 8b and c). We also tested the CIs of these images with StraboTools and it returns an R^2 of 0.86, 0.85 and 0.81 for FeO, SiO_2 and CaO, respectively (Fig. 8d–f). The performance of the average grey level and CI are similar, which is not surprising. This is because both of these indices represent the bulk darkness or lightness of an image. Textural features also correlate with chemical compositions. Among all the texture indices, the best correlation results come from homogeneity, which has an R^2 of 0.82, 0.70 and 0.62 for FeO, SiO_2 and CaO, respectively (Fig. 8g–i). Other texture features of energy, contrast and correlation have R^2 of 0.79, 0.65 and 0.57, respectively for FeO. No correlations were observed between chromatic features (hue and saturation) and chemical compositions.

In Fig. 8, we show the correlations between major oxides and two individual indices, average gray level and homogeneity, extracted from an image. The textural feature has four indices: contrast, correlation, energy and homogeneity. The gray level feature has two indices: mean and standard deviation of gray levels. The chromatic feature has four indices: means and standard deviations of hue and saturation. We explore the use of all these indices in a given feature as well as combining two or more features to predict the chemical compositions of rocks with multivariate linear regression

$$Y = b + a_1x_1 + a_2x_2 + \ldots + a_nx_n \quad (5)$$

where Y is the predicted value, x_i represents the features, and a_i and b are parameters. The parameters can be determined by minimizing the total discrepancy between predicted values and real values. The performances of multivariate linear regression in this study were evaluated based on the 5-fold cross-validation method. In each run, 80% of the data were assigned as a training set and the remaining 20% as the test set. Mean absolute percentage error (MAPE) was used to evaluate model performance:

$$MAPE = \frac{1}{n}\sum_{i}^{n}\left|\frac{A_i - Y_i}{A_i}\right| \quad (6)$$

where A_i is the real value and Y_i is the model-predicted value. MAPE is a measure of relative error and a lower value corresponds to a better model performance.

The results in Table 3 show that the average gray level alone can predict the major oxides of rocks well, which is consistent with our results in Fig. 8. Combining gray level features with chromatic and textural features, however, decreases model performance slightly (Table 3). The robustness of gray level features in predicting composition is not

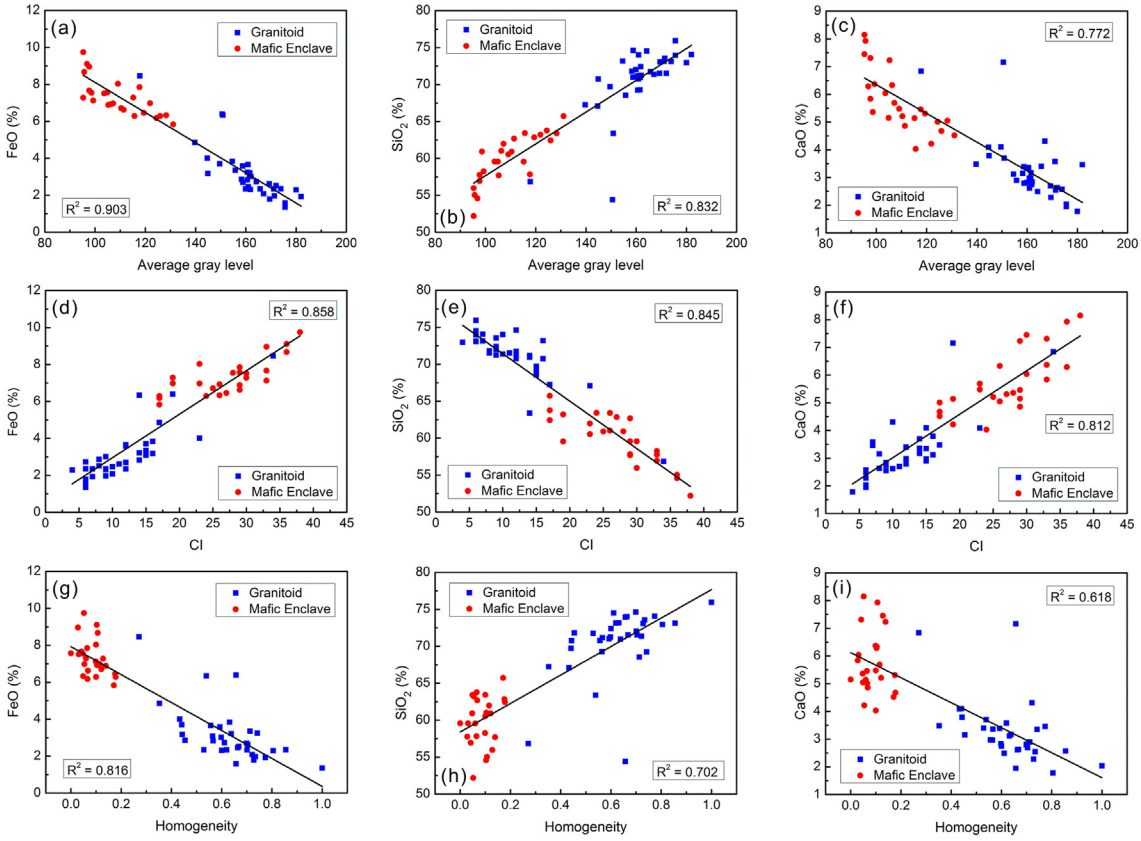

Fig. 8. Correlations between average gray level, CI and homogeneity of calibrated histograms and major element contents from 59 rock samples. Grayscale correlates negatively with whole-rock (a) FeO and (c) CaO, and positively with (b) SiO_2 (wt. %). CI correlates positively with (d) FeO and (f) CaO, and negatively with (e) SiO_2 (wt. %). Homogeneity correlates negatively with (g) FeO and (i) CaO, and positively with (h) SiO_2 (wt. %).

Table 3
Performances (MAPEs) of multivariate linear regression with different features. A lower MAPE means better performance.

Major oxides	Features	Multivariate Linear regression
SiO_2	*Gray level*	0.031
	Chromate	0.054
	Texture	0.049
	Gray level + chromate	0.033
	Gray level + chromate + texture	0.036
CaO	*Gray level*	0.132
	Chromate	0.201
	Texture	0.172
	Gray level+ chromate	0.140
	Gray level + chromate + texture	0.150
FeO	*Gray level*	0.149
	Chromate	0.272
	Texture	0.181
	Gray level + chromate	0.145
	Gray level + chromate + texture	0.157

surprising because granitoid mainly consists of dark (hornblende and biotite) and light minerals (quartz and feldspars), and variations in the proportions of dark to light minerals generally follow bulk chemical compositions. However, weathering effects, which may change the color of minerals (oxidation can generate reddish iron oxide coatings), complicates the use of color, explaining why the use of chromatic features slightly degrades model performance. Chromatic features will no doubt be more useful in rocks with a wider array of colorful minerals, but our work shows that care must be taken to avoid artifacts introduced by weathering or alteration.

Lower model performance when textural features are included is not surprising because textures are not directly controlled by the composition and instead relate to the physical processes by which minerals crystallize or deform. Nevertheless, in our case study of the mafic enclaves and felsic hosts, our results indicate that textural features, for example homogeneity, correlate slightly with composition (Fig. 8g–i). Homogeneity, as used here, accounts for the contrast in gray level between neighboring pixels and the frequency of neighboring pixels that have contrasting gray levels in a given area. Thus, for the same field of view, a fine-grained rock composed of mafic and felsic minerals of contrasting grayscale will be characterized by low homogeneity whereas a coarse-grained rock will be characterized by high homogeneity. Fig. 8g–i shows that homogeneity correlates positively with SiO_2 and negatively with FeO and CaO, indicating that the mafic samples (low SiO_2 and high FeO and CaO) exhibit lower homogeneity than the felsic samples. This result is consistent with the qualitative observation that the mafic enclaves are finer-grained than the felsic hosts. Our results, however, provide a rapid means of quantifying this textural feature. Clearly, textural features should not be used to directly predict bulk rock chemical composition given the superior performance of grayscale in predicting chemical composition. However, our models demonstrate the possibility of rapidly detecting and quantifying any correlations between texture and chemistry, which may have powerful implications for the physico-chemical origin of rocks.

5. Conclusions

In this paper, we proposed a simple but accurate method for imaging and color calibration of rocks using a digital camera on an iPhone 7 Plus. This simple color calibration method, assisted with a color checker as a standard, can greatly improve the consistency of gray level histograms of the rock sample under different light conditions. We also showed that average gray levels of calibrated histograms strongly correlate with the chemical composition of 59 co-genetic plutonic rocks. Our study shows the potential of using image analysis as a rapid means of compositional mapping of plutons. There are no doubt additional challenges associated with uncontrolled field conditions that must be surmounted.

Authorship statement

Julin Zhang: Conceptualization, Color calibration experiments, Python code, Writing - original draft and revision. Cin-Ty A. Lee: Conceptualization, Writing - original draft and revision. Michael Farner: Major element data.

Declaration of competing interest

The authors declare that they have no known competing financial interests or personal relationships that could have appeared to influence the work reported in this paper.

Acknowledgments

We thank Luca Giancardo for his generous advice on image processing. We thank Weidong Sun for handling the manuscript and Francesco Bianconi, Allen Glazner, Xun Yu and three anonymous reviewers for their insightful reviews. Discussions with Ming Tang and Wenrong Cao are appreciated. This work was supported by the U.S. NSF via EAR-1753599.

Appendix.

We first checked the RGB measurements of the color checker to see how light intensity biases color. Fig. A1 shows measured versus actual color for the color checker under CW, W, N, Y and WY light conditions with intensity levels of 1, 5 and 7. Every data point in Fig. A1 represents red (green or blue) measurements corresponding to the 24 calibration standards. Deviations from the 1:1 line indicate measurement bias. All experiments show some level of bias. For Y and WY light conditions, the degree of bias appears to be independent of intensity level (Fig. A1j-o). This is because the iPhone auto exposure program adequately changes exposure time and ISO to compensate for different light intensity. The bias remains constant for CW, W, and N light conditions when intensity increases from level 1 to level 5 (Fig. A1a, b, d, e, g, h), but

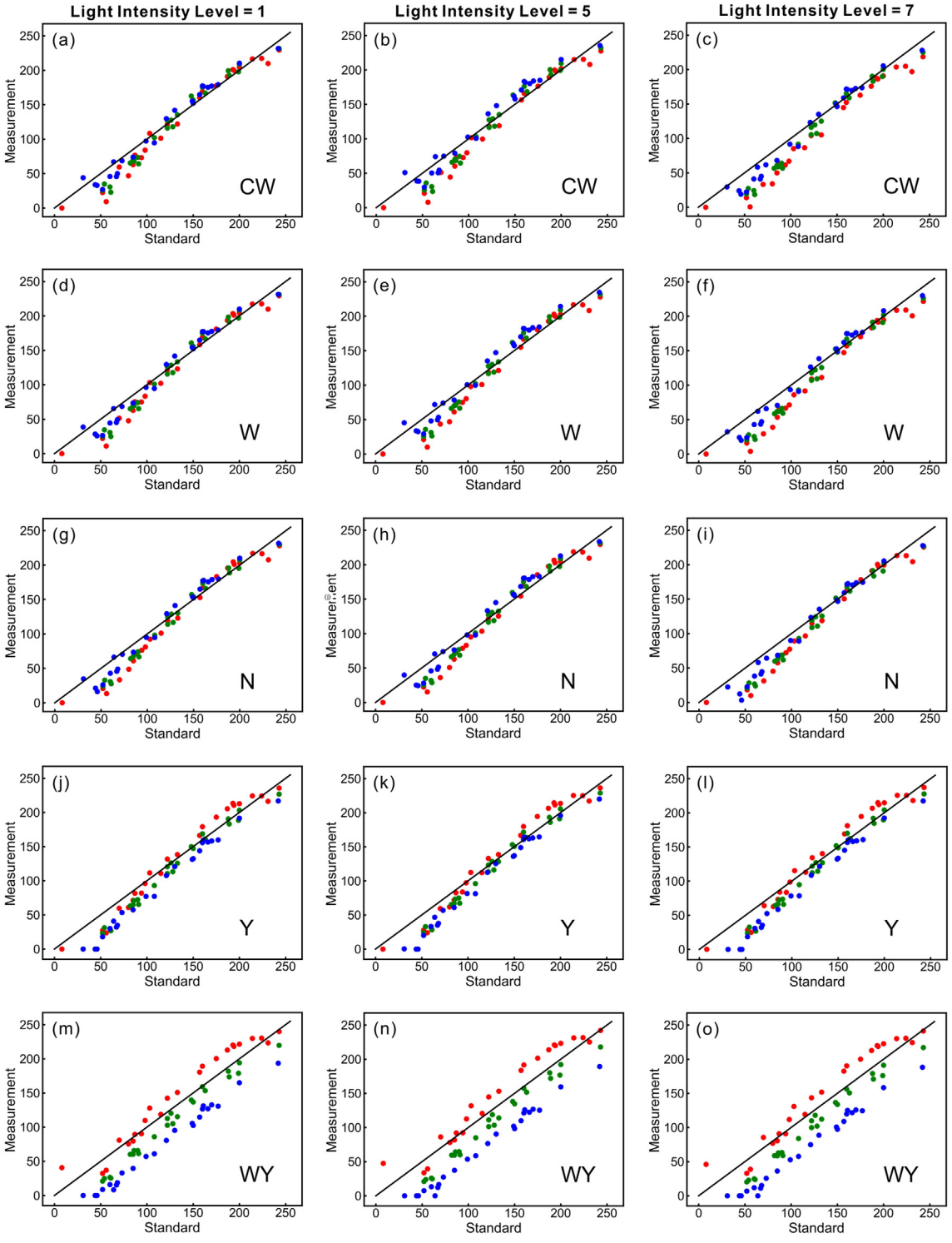

Fig. A1. **Measurement of color-checker standards under different indoor light conditions and intensities.** The X-axis represents standard values and Y-axis represents the measured RGB values. Color (red, green and blue) of each data point refers to the RGB tristimulus value of a particular color patch on the color checker. (a)–(c) CW light, (d)–(f) W light, (g)–(i) N light (j)–(l) Y light, and (m)–(o) WY light. Light intensity was fixed to level 1, 5 and 7 (columns).

when intensity increases to level 7, there is an increase in the negative deviation of measured values compared to standard values (Fig. A1c, f, i).

Of particular interest is how the degree of bias varies between different light conditions, which would indicate that the spectrum of light influences color perception. For an intensity level of 5 (Fig. A1b, e, h, k, n), measurements under CW, W and N mostly fall close to the 1:1 line (Fig. A1b, e, h), with the exception of measurements lower than 100, which fall below the 1:1 line. We also note that the blue data are systematically higher than the green and red data. When Y light is used, some blue data go to zero, indicating underexposure (Fig. A1k).

Unlike CW, W and N light conditions, the red data under Y light conditions are systematically higher than the green and blue data. For WY light, red, green and blue data all show significant bias from the standard (Fig. A1n) although the data parallel the 1:1 line. The color biases observed for the different light conditions are undoubtedly due to differences in the spectrum of the 5 light conditions. CW and W light have more short-wavelength light (blue) but less long-wavelength light (red), so the reflected light of the color checker will have more blue than red light (Fig. A1b, e). In contrast, Y and WY light have more long-wavelength light than short-wavelength light, and as a consequence, the reflected light has more red than blue light (Fig. A1k, n).The above experiments were also used to explore the effects of light intensity and light condition (spectrum) on gray level histograms (Fig. A2, A3). Uncalibrated histograms regardless of light condition are consistent between light intensities of level 1−5 (Fig. A2a, c-f), but shift darker at intensity level of 6 and 7 for CW, W and N light conditions (Fig. A2a, c, d). However, after calibration, histograms converge and are consistent across all light intensities (Fig. A2b). The calibrated histograms become slightly compressed compared to the uncalibrated histograms (Fig. A2a, b).

The effects of light condition on gray level histograms were also explored. Fig. A3a, c, e show the comparisons of uncalibrated gray level histograms for different light conditions under the same light intensity level (1, 4 and 7). The varying light condition caused the centroid of dark and light minerals to migrate. In particular, the light mineral mode in WY light becomes compressed and shifts darker compared to other light conditions, although this effect diminishes when light intensity

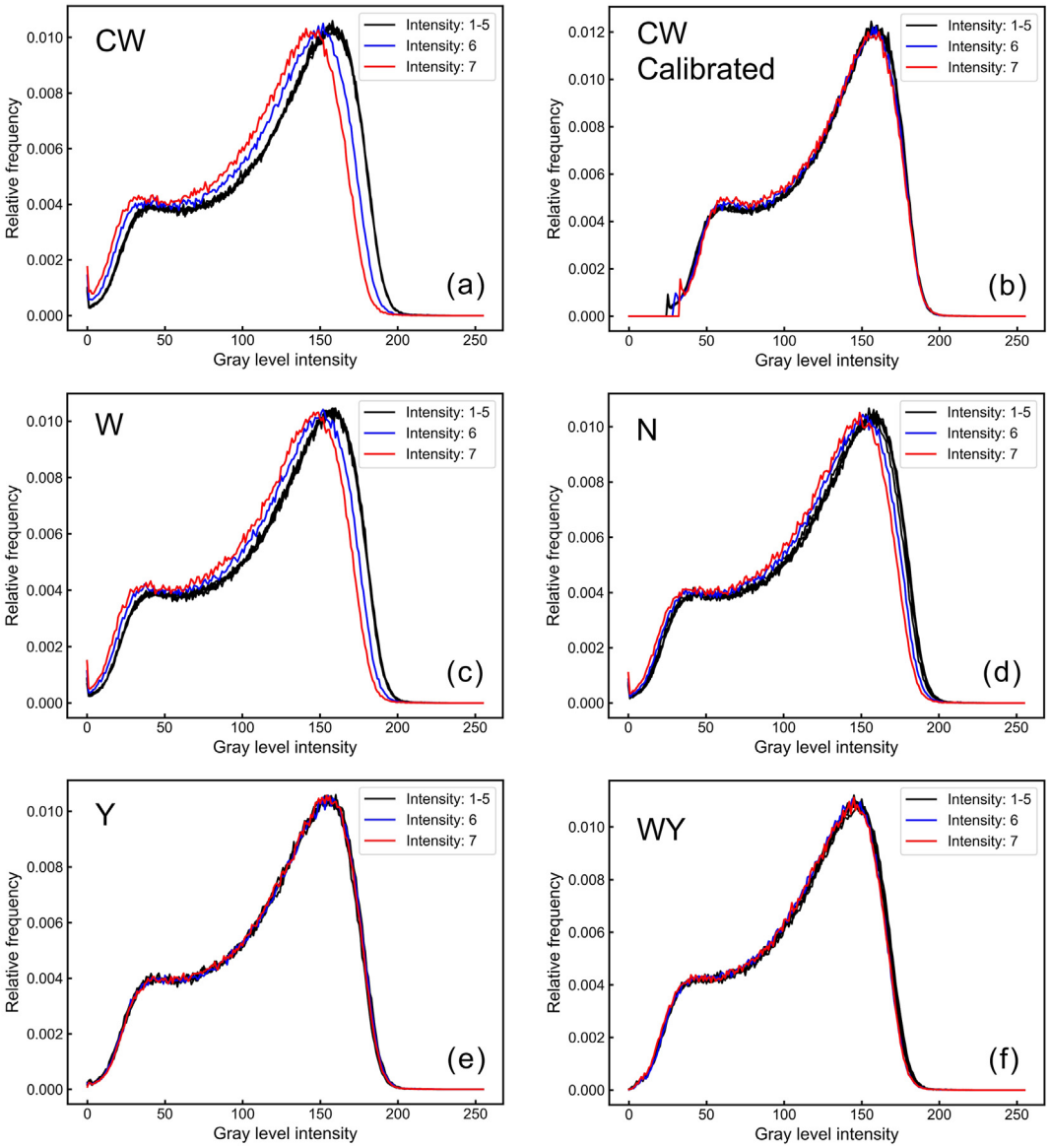

Fig. A2. **Gray level histograms of the rock sample under constant indoor light conditions but different intensities.** (a) Uncalibrated and (b) calibrated histograms under CW light condition with different light intensity levels. Uncalibrated histograms under (c) W, (d) N, (e) Y, and (f) WY light with different light intensity levels.

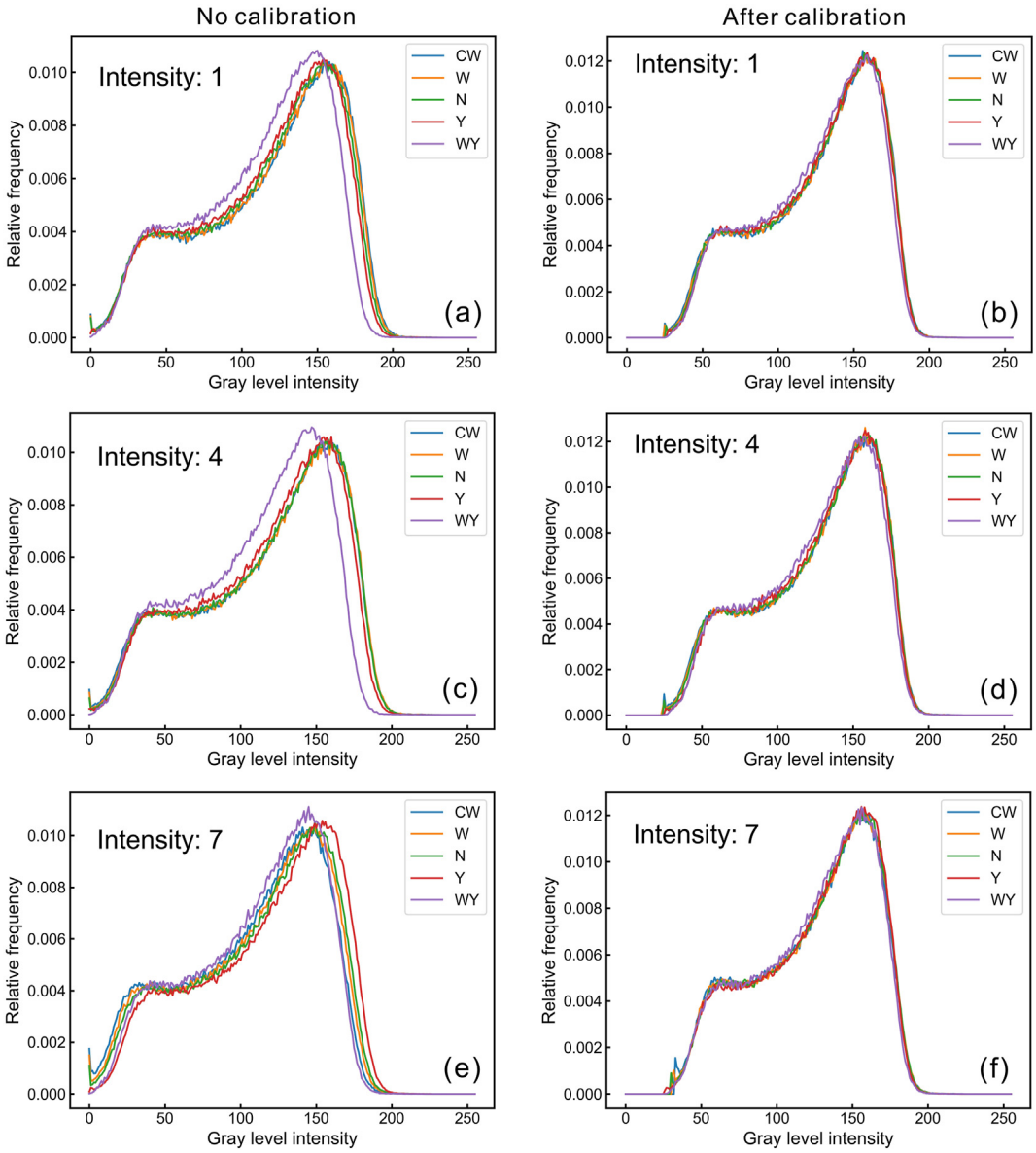

Fig. A3. **Gray level histograms of the rock sample under constant indoor light intensity but different light conditions.** (a) Uncalibrated and (b) calibrated histograms under different light conditions with light intensity fixed to level 1. (c) Uncalibrated and (d) calibrated histograms under different light conditions with light intensity fixed to level 4. (e) Uncalibrated and (f) calibrated histograms under different light conditions with light intensity fixed to level 7.

increases to 7 (Fig. A3e). After calibration, histograms in WY light converge to that of other light conditions (Fig. A3 b, d, f).

Appendix A. Supplementary data

Supplementary data to this article can be found online at https://doi.org/10.1016/j.sesci.2020.12.003.

References

Adams, J.B., Filice, A.L., 1967. Spectral reflectance 0.4 to 2.0 microns of silicate rock powders. J. Geophys. Res. 72, 5705–5715.

Allender, E.J., Stabbins, R.B., Gunn, M.D., Cousins, C.R., Coates, A.J., 2018. The ExoMars spectral tool (ExoSpec): an image analysis tool for ExoMars 2020 PanCam imagery. In: Presented at the Image and Signal Processing for Remote Sensing XXIV. International Society for Optics and Photonics, p. 107890I.

Arvis, V., Debain, C., Berducat, M., Benassi, A., 2004. Generalization of the cooccurrence matrix for colour images: application to colour texture classification. Image Anal. Stereol. 23, 63–72.

Åkesson, U., Stigh, J., Lindqvist, J.E., Göransson, M., 2003. The influence of foliation on the fragility of granitic rocks, image analysis and quantitative microscopy. Eng. Geol. 68, 275–288.

Bianconi, F., González, E., Fernández, A., Saetta, S.A., 2012. Automatic classification of granite tiles through colour and texture features. Expert Syst. Appl. 39, 11212–11218.

Bt, R.I.-R., 2011. Studio Encoding Parameters of Digital Television for Standard 4: 3 and Wide-Screen 16: 9 Aspect Ratios.

Cashman, K.V., Ferry, J.M., 1988. Crystal size distribution (CSD) in rocks and the kinetics and dynamics of crystallization. Contrib. Mineral. Petrol. 99, 401–415.

Cashman, K.V., Marsh, B.D., 1988. Crystal size distribution (CSD) in rocks and the kinetics and dynamics of crystallization II: Makaopuhi lava lake. Contrib. Mineral. Petrol. 99, 292–305.

Color, M., 2015. Munsell soil color charts. Munsell Color.
Costa, C., Pallottino, F., Angelini, C., Proietti, M., Capoccioni, F., Aguzzi, J., Antonucci, F., Menessati, P., 2010. Colour calibration for quantitative biological analysis: a novel automated multivariate approach. Instreument. Viewpt. 70−71.
Doğan, H., Akay, O., 2010. Using AdaBoost classifiers in a hierarchical framework for classifying surface images of marble slabs. Expert Syst. Appl. 37, 8814−8821.
Ershad, S.F., 2011. Color texture classification approach based on combination of primitive pattern units and statistical features. arXiv preprint arXiv: 1109.1133.
Farner, M.J., Lee, C.-T.A., Mikus, M.L., 2018. Geochemical signals of mafic-felsic mixing: case study of enclave swarms in the Bernasconi Hills pluton, California. GSA Bullet. 130, 649−660.
Farner, M.J., Lee, C.-T.A., Putirka, K.D., 2014. Mafic−felsic magma mixing limited by reactive processes: a case study of biotite-rich rinds on mafic enclaves. Earth Planet Sci. Lett. 393, 49−59.
Ferreira, A., Giraldi, G., 2017. Convolutional Neural Network approaches to granite tiles classification. Expert Syst. Appl. 84, 1−11.
Fischer, T., 2019. PCA-based supervised identification of biological soil crusts in multispectral images. Methods 6, 764−772.
Foster, D.H., 2011. Color constancy. Vis. Res. 51, 674−700.
Glazner, A.F., Walker, J.D., 2020. StraboTools: A Mobile App for Quantifying Fabric in Geology.
Gökay, M.K., Gundogdu, I.B., 2008. Color identification of some Turkish marbles. Construct. Build. Mater. 22, 1342−1349.
Haralick, R.M., Shanmugam, K., Dinstein, I.H., 1973. Textural features for image classification. IEEE Trans. Sys. Man. Cybernet. 610−621.
Heilbronner, R., 2000. Automatic grain boundary detection and grain size analysis using polarization micrographs or orientation images. J. Struct. Geol. 22, 969−981.
Hong, G., Luo, M.R., Rhodes, P.A., 2001. A study of digital camera colorimetric characterization based on polynomial modeling, vol. 26. Color Research & Application: Endorsed by Inter-Society Color Council, The Colour Group (Great Britain), Canadian Society for Color, Color Science Association of Japan, Dutch Society for the Study of Color, The Swedish Colour Centre Foundation, Colour Society of Australia, Centre Français de la Couleur, pp. 76−84.
Jerram, D.A., Cheadle, M.J., Philpotts, A.R., 2003. Quantifying the building blocks of igneous rocks: are clustered crystal frameworks the foundation? J. Petrol. 44, 2033−2051.
Joshi, N., Jensen, H.W., 2004. Master's with Distinction in Research Report. Color calibration for arrays of inexpensive image sensors, vol. 30. Stanford University, Department of Computer Science.
Kemeny, J.M., Devgan, A., Hagaman, R.M., Wu, X., 1993. Analysis of rock fragmentation using digital image processing. J. Geptech. Eng. 119, 1144−1160.
Kemp, D.B., 2014. Colorimetric characterisation of flatbed scanners for rock/sediment imaging. Comput. Geosci. 67, 69−74.
Kurmyshev, E.V., Sánchez-Yáñez, R.E., Fernández, A., 2003. Colour texture classification for quality control of polished granite tiles. Proc. Visual. Imag. Imag. Proc. 8−10.
Lepistö, L., Kunttu, I., Visa, A.J., 2005. Rock image classification using color features in Gabor space. J. Electron. Imag. 14, 040503.
Losey Jr., G.S., 2003. Crypsis and communication functions of UV-visible coloration in two coral reef damselfish, Dascyllus aruanus and D. reticulatus. Anim. Behav. 66, 299−307.
Otsu, N., 1979. A threshold selection method from gray-level histograms. IEEE Trans. Sys. Man. Cybernet. 9, 62−66.
Partio, M., Cramariuc, B., Gabbouj, M., Visa, A., 2002. Rock texture retrieval using gray level co-occurrence matrix. In: Presented at the Proc. Of 5th Nordic Signal Processing Symposium. Citeseer.
Pascale, D., 2006. RGB coordinates of the Macbeth Color Checker, 6. The BabelColor Company.
Pendleton, R.L., Nickerson, D., 1951. Soil colors and special Munsell soil color charts. Soil Sci. 71, 35−44.
Perez, C.A., Saravia, J.A., Navarro, C.F., Schulz, D.A., Aravena, C.M., Galdames, F.J., 2015. Rock lithological classification using multi-scale Gabor features from sub-images, and voting with rock contour information. Int. J. Miner. Process. 144, 56−64.
Potts, P.J., 2012. A Handbook of Silicate Rock Analysis. Springer Science & Business Media.
Ran, X., Xue, L., Zhang, Y., Liu, Z., Sang, X., He, J., 2019. Rock classification from field image patches analyzed using a deep convolutional neural network. Mathematics 7, 755.
Romero, J., Hernández Andrés, J., Nieves, J.L., García, J.A., 2003. Color coordinates of objects with daylight changes, vol. 28. Color Research & Application: Endorsed by Inter-Society Color Council, The Colour Group (Great Britain), Canadian Society for Color, Color Science Association of Japan, Dutch Society for the Study of Color, The Swedish Colour Centre Foundation, Colour Society of Australia, Centre Français de la Couleur, pp. 25−35.
Rossel, R.V., Minasny, B., Roudier, P., Mcbratney, A.B., 2006. Colour space models for soil science. Geoderma 133, 320−337.
Stevens, M., Párraga, C.A., Cuthill, I.C., Partridge, J.C., Troscianko, T.S., 2007. Using digital photography to study animal coloration. Biol. J. Linn. Soc. 90, 211−237.
Sullivan, B.L., Aycrigg, J.L., Barry, J.H., Bonney, R.E., Bruns, N., Cooper, C.B., Damoulas, T., Dhondt, A.A., Dietterich, T., Farnsworth, A., 2014. The eBird enterprise: an integrated approach to development and application of citizen science. Biol. Conserv. 169, 31−40.
Topalova, I., Tzokev, A., 2010. Automated texture classification of marble shades with real-time PLC neural network implementation. In: Presented at the 2010 International Joint Conference on Neural Networks (IJCNN). IEEE, pp. 1−8.
Van Horn, G., Mac Aodha, O., Song, Y., Cui, Y., Sun, C., Shepard, A., Adam, H., Perona, P., Belongie, S., 2018. The inaturalist species classification and detection dataset. In: Presented at the Proceedings of the IEEE Conference on Computer Vision and Pattern Recognition, pp. 8769−8778.
Wu, D., Sun, D.-W., 2013. Colour measurements by computer vision for food quality control−A review. Trends Food Sci. Technol. 29, 5−20.